NANO LETTERS

2004
Vol. 4, No. 6
1093−1098

Integration of Colloidal Nanocrystals into Lithographically Patterned Devices

Yi Cui,[†,‡] Mikael T. Björk,[‡] J. Alexander Liddle,[‡] Carsten Sönnichsen,[‡] Benjamin Boussert,[†] and A. Paul Alivisatos*[,†,‡]

Department of Chemistry, University of California, Berkeley, California 94720, and Materials Sciences Division, Lawrence Berkeley National Laboratory, Berkeley, California 94720

Received April 5, 2004

ABSTRACT

We report a facile method for reproducibly fabricating large-scale device arrays, suitable for nanoelectronics or nanophotonics, that incorporate a controlled number of sub-50-nm-diameter nanocrystals at lithographically defined precise locations on a chip and within a circuit. The interfacial capillary force present during the evaporation of a nanocrystal suspension forms the basis of the assembly mechnism. Our results demonstrate for the first time that macromolecule size particles down to 2-nm diameter and complex nanostructures such as nanotetrapods can be effectively organized by the capillary interaction. This approach integrates the merits of bottom-up solution-processed nanostructures with top-down lithographically prepared devices and has the potential to be scaled up to wafer size for a large number of functional nanoelectronics and nanophotonics applications.

Colloidal nanostructures such as metal nanocrystals[1,2] and semiconductor quantum dots,[3,4] nanorods,[5] and nanotetrapods[6] with precisely controlled sizes in the range of 1 to 100 nm exhibit a range of behaviors distinct from those of nanostructures fabricated by vacuum deposition or lithography and are promising building units for nanotechnology. This promise will not be fulfilled, however, unless methods of positioning and addressing these units individually can be developed. Advances in lithography have enabled the precise and reproducible patterning of features from tens of nanometers to the macroscopic scale.[7,8] A synergetic combination of colloidal nanostructures with lithographic patterning can enable the precise control necessary to produce highly integrated nanostructure assemblies on all length scales.[9] Previous efforts in this area have consisted primarily of lithographic patterning followed by random deposition[10,11] or the electrostatic[12] or magnetic[13] trapping of nanostructures. However, these approaches all suffer from some deficiency: they do not provide precise positioning, require specific susceptibilities, have low throughput, and/or are not amenable to scaling.

However, the capillary interaction at the solution interface has been demonstrated to play an important role in driving 2D or 3D crystallization[14−16] and pattern formation[17−20] of micrometer- or millimeter-sized objects and has the potential to be a flexible and high-throughput method. Polymer and silica particles have been successfully organized into lithographically patterned templates[18] by the capillary force, forming highly ordered structures, although the diameters of the particles are typically submicrometer.

It is not obvious whether this approach can be effectively extended to the assembly of sub-50-nm and even sub-10-nm-diameter particles necessary for observing interesting plasmonic and electronic properties because the capillary interaction strength decreases with diminishing object dimension and the randomizing effects of the thermal fluctuation energy (kT) become more significant. A theoretical prediction (ref 21) of the capillary interaction energy between two 2-nm-diameter particles with immersion configuration in water indicates that it is less than kT.

Herein we report that in our scheme, by controlling the appropriate parameters, the capillary force can overcome the random thermal fluctuations to assemble very small nanostructures effectively. We show the reproducible organization of 50-, 8-, and 2-nm-diameter nanoparticles at precise locations on a chip and/or within a circuit. In addition, complex nanostructures such as nanotetrapods and nanostructures of a wide variety of materials are also assembled successfully. Last, we demonstrate the reproducible high-yield fabrication of arrays of single-particle transistors by assembling nanoparticles into electrode gaps. These results imply that it will be possible to move from the study of individual nanoparticle transistors toward the study of arrays of electronically addressable nanoparticles.

Our approach to the controlled assembly of nanostructures exploits capillary interactions with nanostructures at the

* To whom correspondence should be addressed. E-mail: alivis@uclink4.berkeley.edu.
[†] University of California.
[‡] Lawrence Berkeley National Laboratory.

10.1021/nl049488i CCC: $27.50
Published on Web 05/04/2004

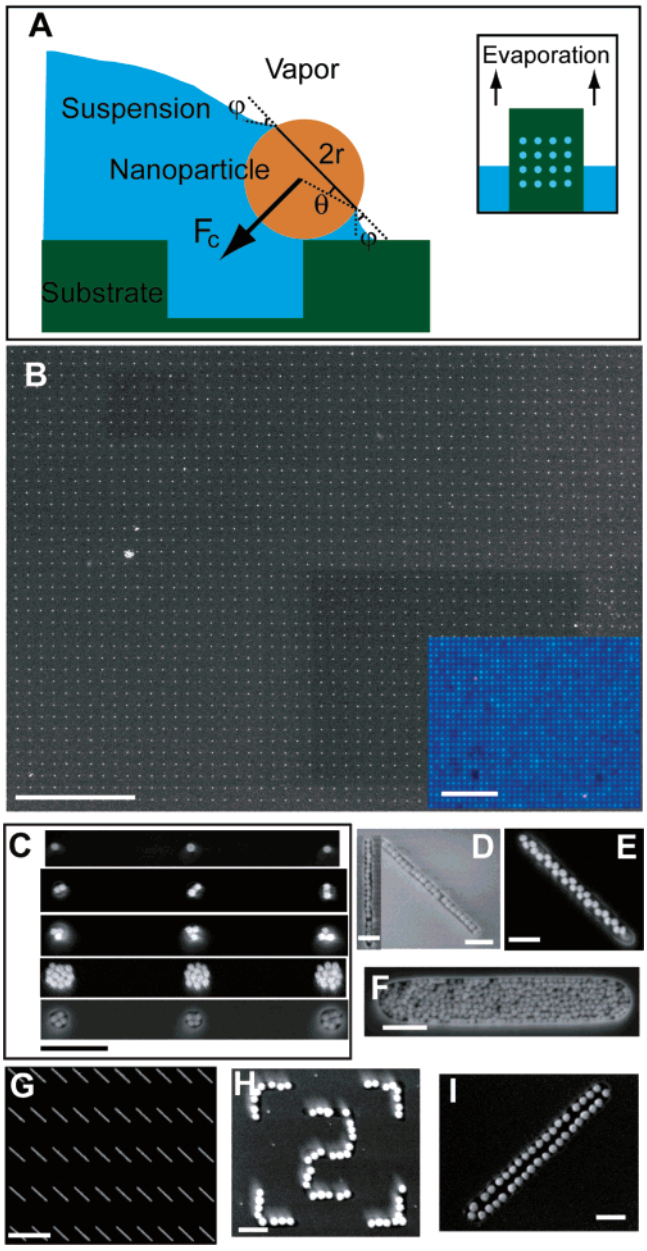

Figure 1. (A) Schematic illustrating the capillary force (F_c) assembly mechanism at the vapor−suspension−substrate three-phase contact line. (Inset) Moving of the three-phase contact line is driven by evaporation in-house vacuum or by heating the solution to ~60 °C. (B) SEM images of 50-nm-diameter Au nanoparticles forming arrays on a hole template substrate. (Inset) White-light scattering image of arrays of single 60-nm Ag nanoparticles. (C) Collection of SEM images of 50-nm particles in holes with different diameters. (D−I) SEM images of 50-nm Au nanoparticles in trenches with different widths or orientations. The templates in C (bottom inset), D, and F are patterned into 300-nm-thick SiO_x, and the templates in other cases are patterned into polymer resist on top of the Au-coated Si substrate. After oxygen plasma, the depth of holes and trenches is ~60 nm. (There is no oxygen plasma treatment in I.) The solution interface moving direction is from bottom to top in all cases. Scale bar: (B) 10 μm, (C) 500 nm, (D, E, H, I) 200 nm, (F) 400 nm, (G) 2 μm.

three-phase vapor−suspension−substrate contact line during controlled solvent evaporation.[22] The basic process is illustrated in Figure 1A. Flat substrates are patterned with hole and trench templates using electron beam lithography and subsequently inserted vertically into a solution containing the nanostructures (Figure 1A inset). The evaporation of the solvent leads to the three-phase contact line moving slowly across the substrate. When the solution film thickness on the substrate is less than the height of the nanostructure, the solution−vapor interface deforms, and the resulting capillary force slides the nanostructure toward the thicker part of the solution and pushes the particle toward the substrate. The net result is that particles are selectively forced into the lithographically defined features as the evaporation zone passes over them but no particles are deposited on the surrounding areas. We note that controlling the contact angle is critical to getting a good assembly of sub-50-nm-diameter particles because it determines the direction of the capillary force and thus the strength of parallel and perpendicular components. The optimal assembly was obtained with the contact angle (see Figure 1 caption) controlled[22] between 10 and 30°, which ensures a large force perpendicular to the substrate capable of overcoming thermal fluctuations and pushing particles into the templates while maintaining the effective sliding action, leading to highly efficient assembly.

We first illustrate the flexibility of this approach using a nearly monodisperse 50-nm-diameter Au nanoparticle aqueous suspension and a Au-coated substrate with patterns in a polymer resist.[22] These particles are in the size range of interesting plasmon properties and can be readily imaged by scanning electron microscopy (SEM). Low-magnification SEM images (Figure 1B) show that the nanoparticles are well organized into 50-nm-diameter hole templates forming single-particle regular arrays controlled precisely by the lithographic design over an area on the order of ~100 × 100 μm^2. White-light scattering (Figure 1B inset) on large-area single-particle arrays shows regular bright dots with a single color, confirming the high regularity and uniformity of the single-particle arrays. We emphasize that the area is limited only by the throughput of the electron beam lithography system: this method is applicable on the wafer scale using other types of lithography such as nanoimprint.[23,24]

There are three key features in this assembly approach: (1) The number of particles deposited in the hole can be controlled over a wide range by varying the ratio of the hole diameter to the diameter of the nanocrystals. For example, we could control the number of 50-nm-diameter nanoparticles in a single hole, from one to two to three or more simply by varying the diameter of the holes (Figure 1C starting from top) from 50, 100, and 110 nm to larger sizes. (2) The combination of self-assembly of particles in the holes and top-down patterning by lithography positions particles precisely into the template and covers multiple length scales in a hierarchical manner. The hole template spacings can be precisely controlled by lithography all the way from 100 nm to the macroscopic scale, and the particle separation and periodicity in a hole can be tuned with different particle sizes and/or core−shell particle structures. (3) This method has very high selectivity for organizing nanoparticles into holes versus other surfaces. To evaluate it in a quantitative way, we define the selectivity parameter by the ratio of the particle

density on these two surfaces. The statistics on a 100 × 100 μm^2 area gives an extremely high selectivity of 10^4. Such a high selectivity is achieved without any additional cleaning steps[11] to remove unwanted nanoparticles and is important for building highly regular arrays and complex structures via multistep processes.

To test whether this assembly method is compatible with current nanoelectronic technology processing on SiO_x−Si substrates, we patterned hole templates into a thick SiO_x layer on top of Si and carried out the assembly process. Figure 1C (bottom inset) clearly demonstrates that nanoparticles were well organized into these templates, with results similar to those obtained with the Au-coated surface patterned with polymer resist. Moreover, the successful and highly selective assembly on the SiO_x surface also confirms that the mechanism of assembly is due to the capillary forces and not to other interactions such as electrostatic or van der Waals forces between the nanoparticles and the substrate because these interactions will cause an indiscriminate deposition of nanoparticles both into hole templates and onto other surfaces.

We notice that the orientations of the particle configuration in most of the holes appear to be random and do not show preferential alignment along the direction of motion of the liquid interface. This suggests that nanoparticles have the freedom to adjust their positions in the holes (Figure 1C). This behavior is different from submicrometer-sized spheres,[18] and we believe that this is because nanoparticles have high mobility in solution and can rearrange their configurations according to the local conditions in the hole immediately after the solution contact line crosses over.

We also implement this method in assembling nanoparticles into extended patterns, which is important for electronics and photonics requiring charge carriers or electromagnetic energy transport over some distance. Figure 1G shows a low-magnification SEM image that demonstrates the close packing of nanoparticles along the whole length of all of the trenches, again with excellent selectivity for the unpatterned substrate area. The configuration can also be controlled by changing the geometric parameters (width, length) of the trenches. When the width of the trench is about the diameter of the nanoparticles, a single-particle chain is obtained (Figure 1D). When the width of the trench is between 1 or 2 times the diameter of the nanoparticles, zigzag-shaped particle chains form (Figure 1E). Chains with a width of several particles are obtained when the trenches are more than twice the nanoparticle diameter (Figure 1F). Because trenches provide a useful test of template anisotropy, we have evaluated the effect of the interface direction of motion with respect to the trench orientation. Trenches with orientations parallel, perpendicular, and 45° to the direction of motion were studied. The results (Figure 1D and inset) show that all orientations have a similar high yield and selectivity, with the relative orientation having no observable effect on assembly. These results are very important because they suggest that it is possible to have structures of arbitrary orientations that will permit the assembly of complex networks for functional applications with a single step.

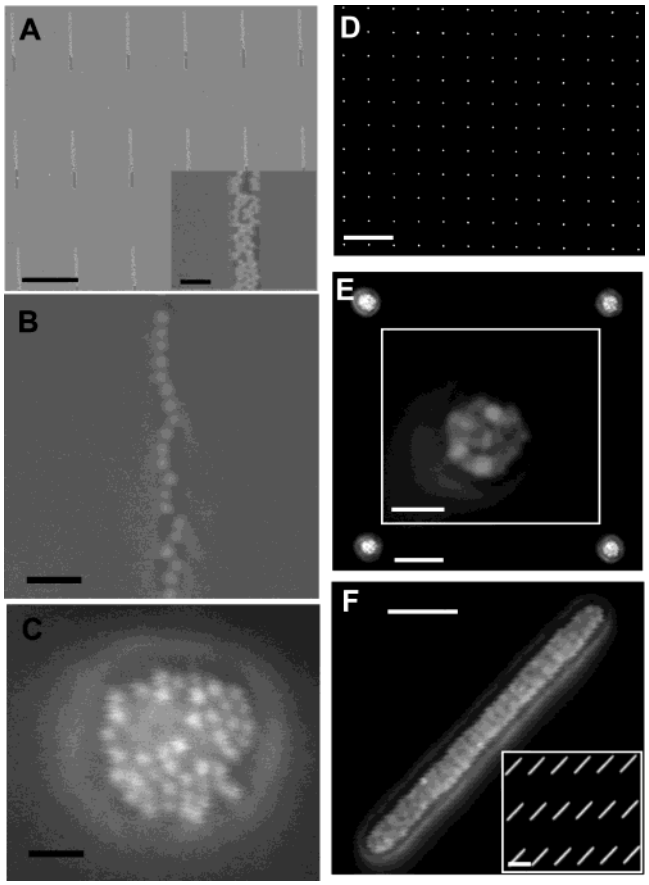

Figure 2. (A−C) SEM images of 8-nm-diameter Au nanoparticles in trenches and holes. The substrates are SiO_x. The depth of the trenches is ∼10 nm. (D−E) SEM images of 2-nm-diameter Au nanoparticles in trenches and holes. The substrates are polymer resist. The depth of the templates is ∼60 nm. The solution interface moving direction in all images is from bottom to top in all cases. Scale bars: (A) 1 μm, inset 50 nm, (B and C) 30 nm, (D) 2 μm, (E and F) 200 nm, (E) inset 50 nm, (F) inset 1 μm.

We have tested this capability by fabricating several different types of complex templates with lithography. After one-step assembly, nanoparticles are placed into complex patterns guided by the templates (as an example shown in Figure 1H). Moreover, this facile way of producing complex patterns can be further strengthened by tuning the substrate surface chemical functionality. For example (Figure 1I), by making trenches hydrophilic and the remaining surface hydrophobic, we are able to induce particles to decorate the edge of large trenches preferentially. This can be understood by considering the pinning of the liquid contact line at the wet trench edge combined with evaporation[25] and the readjustment of nanoparticle positions after the liquid has crossed over the trenches. This is consistent with the previous observation regarding the random orientation of particle assemblies in round holes (Figure 1C).

The highly successful organization of 50-nm-diameter nanoparticles has inspired us to explore the possibility of assembling macromolecule-sized nanostructures with diameters <10 nm, at which quantum confinement effects are manifested. Figure 2A−C shows the organization of 8-nm-diameter Au nanoparticles in trench and hole templates. The yield and selectivity are similar to those of 50-nm nanopar-

ticles. However, it is interesting that the smaller (8 nm) particles do not form such ordered structures as larger ones (50 nm) do in individual templates. We believe that this brings up important questions[26] for further study, namely, how nanoparticle sizes, solvent fluctuations, substrate interactions,, and thermodynamic states affect the drying-pattern formation in a confined geometry. Answering these questions will provide guidelines for the self-assembly of nanodevices. Significantly, this approach can be used to organize nanocrystals as small as 2 nm in diameter. Low-magnification SEM images of 2-nm-diameter Au nanoparticles in 100-nm-diameter hole arrays show the same highly efficient assembly and selectivity into holes seen with the larger particles (Figure 2D). The particles are densely packed in the holes (Figure 2E and inset)—individual particles are hard to resolve because of the limited resolution of the SEM. They can also be assembled effectively into extended trench arrays (Figure 2F and inset).

To understand how efficiently capillary force acts on these smaller particles in our experimental scheme, we performed a rough theoretical estimation (Figure 1A) of the magnitude of the force, $F_c = 2\pi r\sigma \sin \varphi$, where σ is the water−air surface tension, r is particle−water contact-line radius, and φ is the particle−water contact angle, although we have to keep in mind that our continuum physical model might need modification for very small particles because their size is only a few water molecules across. The work done on a particle is approximated by integrating the force for θ from 90 (no solution interface deformation) to 0° (contact-line radius equal to particle radius). Assuming 30° for φ for calculating a lower-bound force and work, the estimated capillary interaction energy is $\sim 24kT$ for 2-nm-diameter particles, suggesting that capillary force is sufficient to overcome thermal fluctuations, consistent with our experimental data. We note that whereas electron beam lithography produces the template size down to about ~20 nm, there are several new approaches[8,27,28] that may make it possible to prepare smaller templates reproducibly so that discrete numbers of 2-nm-diameter particles can also be studied in the future.

We also explored the possibility of assembling anisotropic nanostructures[5,6] because they have unique new properties for nanotechnology. As an example, we investigated the assembly of tetrahedrally shaped CdTe nanotetrapods,[6] which have four nanometer-wide and ~100-nm-long arms that extended three-dimensionally into space. These nanotetrapods provide many unprecedented opportunities for applications, although they also represent much more complex nanostructures for controlled organization than the previous examples.[10−22] Here we show that we could control the assembly of nanotetrapods using our templated capillary force approach. The CdTe nanotetrapods capped by organic surfactant[6] were dissolved in toluene for our study. Figure 3B shows that nanotetrapods are organized into 70-nm-wide trenches with good yield and selectivity although analyzing the details of capillary force on nanotetrapods is more complicated than on spherical nanostructures. In addition to sliding along the surface, there might exist pronounced rotational motion

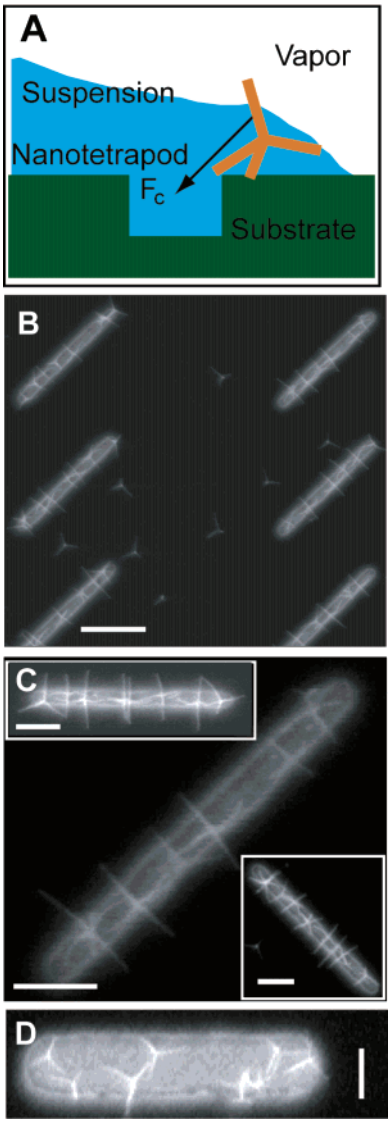

Figure 3. (A) Schematic illustration of nanotetrapods at the three-phase contact line. (B−D) SEM images of CdTe nanotetrapods assembled into trenches. The substrates are polymer on top of Au-coated Si. The depth of the trenches is ~60 nm. There is no oxygen plasma treatment because toluene is used as the solvent. The solution interface moving direction is from bottom to top in all cases. Scale bars: (B) 500 nm, (C and D) 200 nm.

(Figure 3A) in the process. Significantly, nearly all of the nanotetrapods are aligned in the trench, with two arms perpendicular to the trench (projecting out from the substrate) and the other two parallel (projecting into the trench) (Figure 3C and insets). Their assembly is also independent of the trench orientation relative to the solution dewetting direction. We found, however, that the alignment becomes less perfect as the trenches become wider. As shown in Figure 3D, the alignment is essentially random for 220-nm-wide trenches, which is larger than the overall dimension of tetrapods. These observations suggest that the alignment is due to the spatial confinement of two nanotetrapod arms by the trench width and improved alignment could, in principle, be obtained using extremely narrow trenches with a width approximately equal to the diameter of the arms. The organization of CdTe nanotetrapods extends this assembly method to semiconduc-

tors, suggesting that it can be applied to nanostructures of any material because the capillary force is material-independent. This technique is therefore generic, unlike electrical or magnetic assembly,[12,13] which relies on the specific susceptibility of certain materials. Note that the arms of the tetrapods in the trenches are plastically deformed when the last solvent in the trench evaporates, pressing the tetrapods against the walls. Further study of this deformation of nanotetrapods versus arm length and width is underway and may lead to a quantitative understanding of the magnitude of the capillary forces responsible for nanoparticle assembly.

The power of this approach can be extended in many directions. For example, many of the current nanoelectronic devices[10] have been prepared by randomly depositing nanostructures into the gap between two electrodes, which is a low-yield and uncontrolled process. We demonstrate that controllable high-yield assembly of nanostructures between electrodes can be realized by our approach. Figure 4A shows our strategy for electronic device fabrication: prefabricated electrode pairs with a gap ~50 nm are covered with a layer of polymer resist, and a small trench window is opened by lithography right onto the gap of each pair of electrodes, followed by a capillary assembly process of 50-nm Au nanoparticles and lift-off of polymer for imaging (Figure 4A). SEM images on a large area (Figure 4B) show that more than 90% of the electrode pairs have a single particle in the gap, which is significantly better than the random deposition method (typical yield of a few percent). Higher-magnification SEM images (Figure 4C) show that single particles are connected well with electrodes and that there is also one particle on top of each electrode, consistent with our assembly schematic in Figure 4A. This therefore provides a method to produce well-defined samples for further electrical transport measurements of nanocrystals and their assemblies (Figure 4 caption). Room-temperature electrical transport measurements through single nanoparticles (Figure 4D) show that most of our devices have nonlinear current versus voltage ($I-V$) behavior with zero-bias resistance from 100 MΩ to GΩ, suggesting that the contact is of the high-resistance tunneling type necessary for investigating many mesoscopic phenomena such as single-electron charging. Measurements on the same device through at least 100 cycles show reproducible $I-V$ characteristics (Figure 4D, dashed line) and indicate reliable stable contact formation. The substrate backgate-dependence measurements at room temperature do not show any gate response, consistent with the fact that the particles are metallic and their size is not small enough to see single-electron charging at room temperature. Although the size (50 nm) of single particles is limited by the electrode gap in the current experiment, the method[27] for making electrodes with nanometer separation will be exploited such that single-electron and quantum behaviors in single nanometer-sized particles can be studied.

In summary, our studies have delineated a facile and powerful approach for the hierarchical assembly of isotropic and anisotropic colloidal nanostructures over large areas and represent a significant step toward the integration of bottom-up chemically prepared nanostructures with lithographically patterned nanostructures. The research enabled by this approach could directly lead to highly integrated functional nanosystems. For example, tunable plasmon waveguides made of metal nanocrystal chains for nanophotonics[29] are

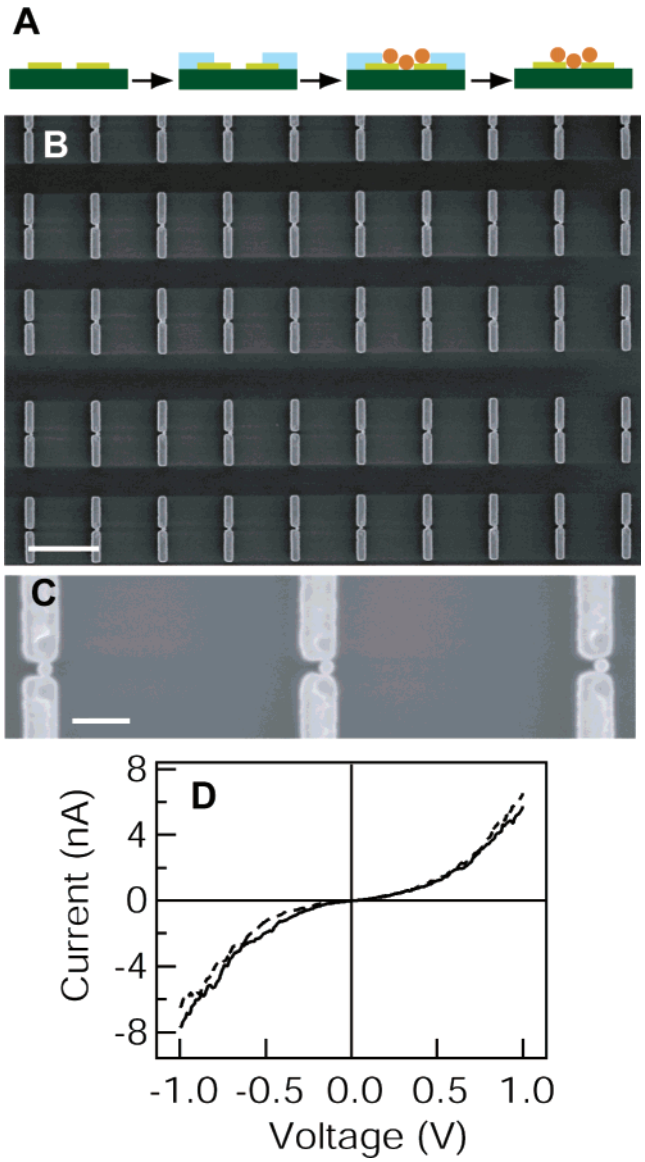

Figure 4. (A) Schematic of the fabrication process: the prefabricated electrode pairs (yellow) on oxide substrates (green) with gaps of ~50 nm were coated with polymethyl methacrylate (PMMA) resist (blue), and windows were opened onto the gaps by electron beam lithography, followed by capillary force assembly of 50-nm-diameter Au nanoparticles (orange). The resist was removed using acetone for SEM imaging. (B) Low-magnification SEM image of single 50-nm Au nanoparticles organized between pairs of electrodes over a large area. (C) High-magnification SEM image on part of B. The solution interface moving direction is from bottom to top in all cases. Scale bar: (B) 1 μm, (C) 200 nm. (D) Plot of typical current (I) versus electrode bias voltage (V) behaviors of the single-particle devices. The dashed line is the measurement data after 100 cycles. The electrical devices were made by doing one more step of lithography on the sample in B to connect the small electrodes to an outside bonding pad for measurements. Annealing PMMA resist at 120 °C for 1 h was usually performed for lithography, which might also partially account for forming stable contacts between nanoparticles and electrodes.

currently under investigation. Highly integrated single-electron transistor arrays could be readily assembled using small nanoparticles, which could perform electrical functions even at room temperature.[30] Moreover, this assembly method can be applied to nanostructures of any material, and the designed combination of chemically distinct nanostructures through multistep organization could increase both the structural and functional complexity for highly integrated, multifunction applications.

Acknowledgment. We thank D. Ah Tye for help with SEM and Professor U. Banin, Professor P. Geissler, and Dr. Y. Yin for helpful discussions. We also thank the National Center for Electron Microscopy at Lawrence Berkeley National Laboratory and the UC Berkeley Microfabrication Laboratory for the use of their facility. Y.C. thanks the Miller Institute for a fellowship. This work was supported by the Director, Office of Science, Office of Basic Energy Sciences, Division of Materials Sciences and Engineering of the U.S. Department of Energy under contract no. DE-AC03-76SF00098 and by the Department of Defense Advanced Research Projects Agency under award no. 066995.

References

(1) Brust, M.; Kiely, C. J. *Colloids Surf., A* **2002**, *202*, 175−186.
(2) Mirkin, C. A. *Inorg. Chem.* **2000**, *39*, 2258−2272.
(3) Alivisatos, A. P. *Science* **1996**, *271*, 933−937.
(4) Murray, C. B.; Kagan, C. R.; Bawendi, M. G. *Annu. Rev. Mater. Sci.* **2000**, *30*, 545−610.
(5) Peng, X.; Manna, U.; Yang, W.; Wickham, J.; Scher, E.; Kadaranich, A.; Alivisatos, A. P. *Nature* **2000**, *404*, 59−61.
(6) Manna, L.; Milliron, D. J.; Meisel, A.; Scher, E. C.; Alivisatos, A. P. *Nature Mater.* **2003**, *2*, 382−385.
(7) Ito, T.; Okazaki, S. *Nature* **2000**, *406*, 1027−1031.
(8) Marrian, C. R. K.; Tennant, D. M. *J. Vac. Sci. Technol., A* **2003**, *21*, S207−215.
(9) Whitesides, G. M.; Grzybowski, B. *Science* **2002**, *295*, 2418−2421.
(10) Klein, D. L.; Roth, R.; Lim, A. K. L.; Alivisatos, A. P.; McEuen, P. L. *Nature* **1997**, *389*, 699−701.
(11) Spatz, J. P.; Chan, V. Z.-H.; Mö*ß*mer, S.; Kamm, F.-M.; Plettl, A.; Ziemann, P.; Möller, M. *Adv. Mater.* **2002**, *14*, 1827−1832.
(12) Bezryadin, A.; Dekker, C.; Schmid, G. *Appl. Phys. Lett.* **1997**, *71*, 1273−1275.
(13) Lee, C. S.; Lee, H.; Westervelt, R. M. *Appl. Phys. Lett.* **2001**, *79*, 3308−3310.
(14) Denkov, N. D.; Velev, O. D.; Kralchevsky, P. A.; Ivanov, I. B.; Yoshimura, H.; Nagayama, K. *Nature* **1993**, *361*, 26.
(15) Jiang, P.; Bertone, J. F.; Hwang, K. S.; Colvin, V. L. *Chem. Mater.* **1999**, *11*, 2132−2140.
(16) Vlasov, Y. A.; Bo, X.; Sturm, J. C.; Norris, D. J. *Nature* **2001**, *414*, 289−293.
(17) Aizenberg, J.; Braun, P. V.; Wiltzius, P. *Phys. Rev. Lett.* **2000**, *84*, 2997−3000.
(18) Yin, Y.; Lu, Y.; Gates, B.; Xia, Y. *J. Am. Chem. Soc.* **2001**, *123*, 8718−8729.
(19) Nikolaides, M. G.; Bausch, A. R.; Hsu, M. F.; Dinsmore, A. D.; Brenner, M. P.; Gay, C.; Weltz, D. *Nature* **2002**, *420*, 299−301.
(20) Bowden, N. B.; Weck, M.; Choi, I. S.; Whitesides, G. M. *Acc. Chem. Res.* **2001**, *34*, 231−238.
(21) Kralchevsky, P. A.; Nagayama, K. *Adv. Colloid Interface Sci.* **2000**, *85*, 145−192.
(22) There were two types of substrates used in our study: 50-nm Au-coated Si substrates and 300-nm SiO_x on top of Si. Both types of substrates were spin coated with 80-nm-thick KRS-XE polymer resist (JSR Corp.) and patterned using electron beam lithography. The Au-coated substrates were used after developing, and thus the bottom of the templates is Au and the side wall is polymer resist. For the SiO_x substrate, after electron beam lithography, the hole patterns are transferred from the resist to the oxide layer by reactive ion etching, and thus the bottom and side walls of the templates are SiO_x. For both substrates, a short oxygen plasma treatment was used (except in Figure 1 (**I**) and Figure 3) to produce surfaces with contact angles between 10 and 30° before inserting into an Au or Ag aqueous suspension (Ted Pella Inc.) with a concentration of 4.5×10^{10} to 10^{12} particles/mL. The moving of the three-phase contact line is driven by evaporation in-house vacuum or heating the solution to ∼60 °C.
(23) Zhang, W.; Chou, S. Y. *Appl. Phys. Lett.* **2003**, *83*, 1632−1634.
(24) Bailey, T. C.; Johnson, S. C.; Sreenivasan, S. V.; Ekerdt, J. G.; Willson, C. G.; Resnick, D. J. *J. Photopolym. Sci. Technol.* **2002**, *15*, 481−486.
(25) Su, G.; Guo, Q.; Palmer, R. E. *Langmuir* **2003**, *19*, 9669−9671.
(26) Rabani, E.; Reichman, D. R.; Geissler, P. L.; Brus, L. E. *Nature* **2003**, *426*, 271−274.
(27) Park, H.; Lim, A. K. L.; Alivisatos, A. P.; Park, J.; McEuen, P. L. *Appl. Phys. Lett.* **1999**, *75*, 301−303.
(28) Choi, Y.; Zhu, J.; Grunes, J.; Bokor, J.; Somorjai, G. A. *J. Phys. Chem. B* **2003**, *107*, 3340−3343.
(29) Maier, S. A.; Brongersma, M. L.; Kik, P. G.; Meltzer, S.; Requicha, A. A. G.; Atwater, H. A. *Adv. Mater.* **2001**, *13*, 1501−1505.
(30) Grabert, H.; Devoret, M. H. *Single Charge Tunneling: Coulomb blockade phenomena in nanostructures* (Plenum Press: New York, 1992).

NL049488I